



Electrically controllable thermal transport in Josephson junctions based on buckled two-dimensional materials

Yu-Hao Zhuo, Biao Wu, Gang Ouyang , and Hai Li *

Key Laboratory of Low-Dimensional Quantum Structures and Quantum Control of Ministry of Education, Key Laboratory for Matter Microstructure and Function of Hunan Province, School of Physics and Electronics, Hunan Normal University, Changsha 410081, China



(Received 5 February 2023; revised 30 June 2023; accepted 1 September 2023; published 13 September 2023)

We investigate the thermal transport properties in superconductor-antiferromagnet-superconductor and superconductor-ferromagnet-superconductor junctions based on buckled two-dimensional materials (BTDMs). Owing to the unique buckled sublattice structures of BTDMs, in both junctions the phase dependence of the thermal conductance can be effectively controlled by perpendicular electric fields. The underlying mechanism for the electrical tunability of thermal conductance is elucidated resorting to the band structures of the magnetic regions. We also reveal the distinct manifestations of antiferromagnetic and ferromagnetic exchange fields in the thermal conductance. These results demonstrate that the perpendicular electric field can serve as a knob to externally manipulate the phase-coherent thermal transport in BTDMs-based Josephson junctions.

DOI: [10.1103/PhysRevB.108.115417](https://doi.org/10.1103/PhysRevB.108.115417)

I. INTRODUCTION

The thermal transport in temperature-biased Josephson junctions has recently garnered considerable attention, due to the extensive applications ranging from phase-coherent caloritronics [1–13] to the detection of novel quantum states [14–22]. In Josephson junctions, the formation of Andreev-bound states (ABSs) has a profound impact on the quasiparticle scattering. Since the binding energy and spectral weight of the ABSs depend on the superconducting phase difference, the coupling between the quasiparticles and ABSs gives rise to a phase-coherent component of the thermal current [23–26]. This effect holds the promise to manipulate the thermal transport via the phase coherence intrinsic to superconducting condensates, boosting the efforts to design phase-coherent caloritronics devices based on Josephson junctions [1–6]. During the last decade, there has been tremendous experimental progress in the realm of phase-coherent caloritronics. Renowned examples include the heat interferometer [2], heat modulator [3], thermal router [4], and thermal $0 - \pi$ phase transition [5] realized in temperature-biased Josephson junctions.

On the other hand, since the thermal currents are mainly carried by quasiparticles with energies above the superconducting gap, they provide complementary information to the charge currents which derive essentially from the ABSs or quasiparticles with energies below the superconducting gap [14,23–27]. In this regard, the thermal transport measurement opens an alternative route to identify the existence of novel quantum states. Recent theoretical proposals have shown that the thermal currents in temperature-biased topological Josephson junctions can be used to probe the topological ABSs [14], Majorana zero modes [15,16], Jackiw-Rebbi

resonant states [17], and helical edge states [18,19]. Furthermore, since the thermal transport is sensitive to the pairing symmetry of the superconducting condensate, the thermal transport signature offers a viable way to distinguish the spin-singlet and spin-triplet pairing states in temperature-biased topological [20] and conventional Josephson junctions [22].

Although significant achievements have been made in the thermal transport properties of Josephson junctions, the research attention to date has mainly been restricted to the phase-coherent aspect of thermal transport [2–10,13–26]. In practice, the manipulation of the proposed phase dependence needs to resort to an external magnetic field [2–6]. It is natural to ask whether the phase-coherent thermal transport can be managed in a fully electric manner. An exciting possibility is to consider the thermal transport in Josephson junctions based on buckled two-dimensional materials (BTDMs) which harbor electrically tunable low-energy physics.

BTDMs, referring to silicene, germanene, and stanene, are atomically thin crystals possessing honeycomb lattices and Dirac-like low-energy excitations [28–40]. It has been demonstrated that a stable BTDM sheet prefers a buckled sublattice structure, where the two sublattices A and B are separated from each other in the direction perpendicular to the sheet plane [35–38], i.e., the z direction, as shown in Fig. 1. Owing to the broken sublattice symmetry, a staggered sublattice potential can be generated by applying a perpendicular electric field along the z direction [39,40]. Consequently, the low-energy bands and relevant transport properties can be effectively modulated by the perpendicular electric field [39–46]. Moreover, recent diversified efforts have predicted that superconducting correlations can be induced in BTDMs through the proximity effect [47–50]. These advances, together with the unique buckled geometry, render BTDMs fertile playgrounds to explore the electrically tunable phase-coherent transport properties [51–58]. One of the most prominent examples is the occurrence of electrically

*hnuhl@hunnu.edu.cn

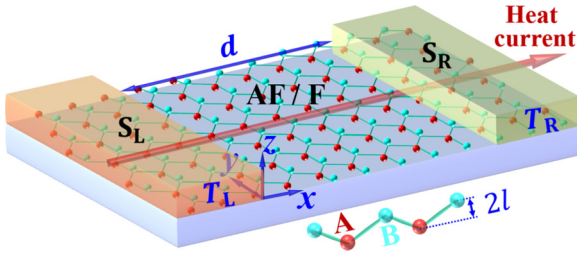


FIG. 1. Sketch of a BTDM-based Josephson junction with a heat current flowing along the x direction. The BTDM sheet consists of a monolayer of X atoms ($X=\text{Si, Ge, or Sn}$) arranging in a two-dimensional honeycomb lattice, where the two triangular sublattices A (red) and B (cyan) are separated from each other by a distance $2l$ in the z direction.

controlled $0 - \pi$ phase transition in silicene-based Josephson junctions [52–54]. Additionally, recent progress has also revealed that both the local and nonlocal Andreev reflections in silicene-based superconducting hybrid structures can be regulated by a perpendicular electric field [50,55–57]. However, up to now the effects of perpendicular electric field on the phase-coherent thermal transport have been scarcely studied in BTDMs-based Josephson junctions.

Motivated by the significance but the lack of detailed understanding about the electrically tunable thermal transport in Josephson junctions, in this paper we investigate the thermal transport properties in superconductor-antiferromagnet-superconductor (S-AF-S) and superconductor-ferromagnet-superconductor (S-F-S) junctions based on BTDMs. Since the perpendicular electric field can modulate the band structures of BTDMs, the phase dependence of thermal conductance is electrically controllable in both S-AF-S and S-F-S junctions. Taking advantage of the band structures in the magnetic regions, the electrical tunability of phase-coherent thermal conductance is elucidated. We also illustrate the different manifestations of antiferromagnetic and ferromagnetic exchange fields in the thermal conductance. Our work suggests that the perpendicular electric field can be put forward as a knob to manipulate the phase-coherent thermal transport in BTDMs-based Josephson junctions.

This paper is structured as follows. We present the model and calculation method in Sec. II. In Sec. III, we give the numerical results and discuss the effects of the perpendicular electric field on the thermal conductance. Finally, the conclusion is briefly drawn in Sec. IV.

II. MODEL AND APPROACH

A schematic of the proposed Josephson junction is shown in Fig. 1, where a BTDM sheet is deposited in the xy plane, with two superconducting electrodes S_L and S_R , respectively, covering the left-hand (L, $x < 0$) and right-hand (R, $x > d$) sides of the junction. To drive a thermal current flowing along the x direction, a temperature gradient is imposed across the junction, where the temperature in the L (R) region is fixed as $T_{L(R)}$ with $T_{L(R)} = T + (-)\delta T/2$. The superconductivity in the L and R regions can be induced by the s -wave superconducting electrodes via the proximity effect, as that has been experimentally carried out in

similar two-dimensional materials such as graphene [59–63] and transition-metal dichalcogenides [64,65]. In the magnetic region (M, $0 < x < d$) of the S-AF-S (S-F-S) junction, an antiferromagnetic (ferromagnetic) exchange field is introduced to regulate the thermal transport. As demonstrated by recent experiments, the proposed exchange fields can be realized in BTDMs by intercalating rare-earth atoms [66,67].

In the superconducting regions, we consider the same model as in Ref. [50] and neglect the intersublattice pairing for simplicity. Accordingly, in the basis of $\psi_k^\dagger = \{(\psi_{k,\sigma}^A)^\dagger, (\psi_{k,\sigma}^B)^\dagger, \psi_{-k,\bar{\sigma}}^A, \psi_{-k,\bar{\sigma}}^B\}$ spanned in the Nambu \otimes sublattice space, the Bogoliubov–de Gennes (BdG) Hamiltonian is given by [50–54]

$$\mathcal{H} = \begin{pmatrix} H_0 - \sigma h & \sigma \Delta \\ \sigma \Delta^\dagger & -(H_0 - \bar{\sigma} h) \end{pmatrix}, \quad (1)$$

where the spin index $\sigma = \pm 1$ satisfies $\sigma = -\bar{\sigma}$. The single-particle effective Hamiltonian $H_0 = \hbar v_F (\eta k_x \tau_x - k_y \tau_y) + m_{\eta\sigma} \tau_z - \mu \tau_0$ [39–46]. In our notation, τ_j ($j = x, y, z$) denotes the Pauli matrix in the sublattice space, τ_0 is a 2×2 unit matrix, v_F represents the Fermi velocity, and $\eta = +(-)1$ labels the $K(K')$ valley. The effective-mass term $m_{\eta\sigma} = lE_z - \eta\sigma\lambda_{\text{SO}}$, where λ_{SO} indicates the strength of spin-orbit coupling, E_z parameterizes the perpendicular electric field, and $2l$ is the separation between the A and B sublattices along the z direction. In the S-AF-S and S-F-S junctions, the exchange fields are, respectively, characterized as $h = h_{\text{AF}} \tau_z \Theta(x) \Theta(d-x)$ and $h = h_{\text{F}} \tau_0 \Theta(x) \Theta(d-x)$, with $\Theta(x)$ the Heaviside step function. The chemical potential $\mu = \mu_S \Theta(-x) + \mu_M \Theta(x) \Theta(d-x) + \mu_S \Theta(x-d)$. In this paper, we take the superconducting regions to be heavily doped to satisfy the relation of $\mu_S \gg \mu_M$, so that the leakage of Cooper pairs from the superconducting regions to the magnetic region can rationally be neglected [50–58]. In doing so, the superconducting gap can be effectively modeled by a step function, i.e., $\Delta = \Delta_L(T_L) \tau_0 e^{i\phi_L} \Theta(-x) + \Delta_R(T_R) \tau_0 e^{i\phi_R} \Theta(x-d)$, with the phase difference being defined as $\phi = \phi_R - \phi_L$. The amplitude of the superconducting gap is given by $\Delta_{L(R)}(T_{L(R)}) = \Delta_0 \tanh(1.74\sqrt{T_C/T_{L(R)} - 1})$, where the critical temperature $T_C = \Delta_0/(1.76k_B)$ and k_B denotes the Boltzmann constant [8,11]. We notice that although the consequences resulting from the employed step-function-like potentials may quantitatively deviate from the measurements caused by experimentally available potential profiles, the physical pictures and main results on the electrically tunable phase-coherent thermal transport, given by the two types of potential profiles, should be essentially the same, as that has been extensively demonstrated in a large amount of similar superconducting hybrid structures [9–22,49–58,62,63].

In the present work, we study the thermal transport properties by adopting the scattering wave approach. This method has been extensively employed to investigate the thermal transport properties in temperature-biased superconducting hybrid structures [9–22,27]. As compared to the approaches of tunneling Hamiltonian and Usadel equations in quasiclassical approximation, the scattering wave method possesses the advantage to explore the thermal transport properties in single- or few-channel superconducting hybrid structures with arbitrary transparency [12].

To evaluate the thermal conductance in the proposed Josephson junctions, we first compute the quasiparticle transmission probabilities. For an electronlike (a holelike) quasiparticle incident from the L region, the resulting wave function $\Psi_L^{e(h)}$ is given by

$$\Psi_L^{e(h)} = \psi_{eq(hq)}^{L,+} + r_{\eta\sigma}^{ee(hh)} \psi_{eq(hq)}^{L,-} + r_{\eta\sigma}^{he(eh)} \psi_{hq(eq)}^{L,-}, \quad (2)$$

where $r_{\eta\sigma}^{ee,hh}$ and $r_{\eta\sigma}^{he,eh}$ denote the valley- and spin-resolved scattering amplitudes of normal reflections and Andreev reflections, respectively. The corresponding wave function in the R region is formulated as

$$\Psi_R^{e(h)} = t_{\eta\sigma}^{ee(hh)} \psi_{eq(hq)}^{R,+} + t_{\eta\sigma}^{he(eh)} \psi_{hq(eq)}^{R,+}, \quad (3)$$

with $t_{\eta\sigma}^{ee,hh,he,eh}$ the valley- and spin-resolved transmission amplitudes. The details of electronlike (holelike) scattering states $\psi_{eq(hq)}^{L,\pm}$ and $\psi_{eq(hq)}^{R,\pm}$ are presented in Appendix. In the M region, the wave function Ψ_M is a linear superposition of all possible scattering states, i.e.,

$$\Psi_M = c_1 \psi_e^+ + c_2 \psi_e^- + c_3 \psi_h^+ + c_4 \psi_h^-, \quad (4)$$

where the scattering amplitudes are denoted by c_j ($j = 1, 2, 3, 4$) and the explicit expressions of scattering states $\psi_{e,h}^\pm$ are given in Appendix.

The transmission amplitudes can be obtained by matching the relevant wave functions at boundaries $x = 0$ and $x = d$. In general, at the boundaries there inevitably exist interfacial imperfections such as the structural-deformation-induced lattice mismatch resulting from the distinct dressing effects caused by the magnets and superconducting electrodes. To take into account the influences engendered from the interfacial imperfections, at the boundary $x = 0$ (d) we place an ultranarrow square potential barrier characterized by strength $U_{L(R)}$ and width $\ell_{L(R)}$, and then take the limits of $U_{L(R)} \rightarrow \infty$ and $\ell_{L(R)} \rightarrow 0$ with $U_{L(R)}\ell_{L(R)}/(\hbar v_F) \equiv Z_{L(R)}$ being finite [14,27]. Parenthetically, the proposed interfacial potential barriers can also model the effects of ultranarrow insulating layers located at the boundaries [55,58]. According to the conservation of the particle current flowing along the x direction, the boundary conditions can be formulated as

$$\Psi_L^{e(h)}|_{x=0^-} = \mathcal{M}_L^{-1} \Psi_M|_{x=0^+}, \quad (5a)$$

$$\Psi_R^{e(h)}|_{x=d^+} = \mathcal{M}_R \Psi_M|_{x=d^-}, \quad (5b)$$

with the transfer matrix $\mathcal{M}_{L(R)}$ being defined as

$$\mathcal{M}_{L(R)} = e^{i\nu_0 \tau_x \eta Z_{L(R)}}, \quad (6)$$

where ν_0 denotes a unit matrix operating in the Nambu space.

With the aid of the transmission amplitudes, the total valley- and spin-resolved transmission probability resulting from the electronlike and holelike incident quasiparticles can be obtained as

$$\mathcal{T}_{\eta\sigma}(\epsilon, \theta) = \left| \frac{\langle \psi_{eq}^{R,+} | \hat{j}_x | \psi_{eq}^{R,+} \rangle}{\langle \psi_{eq}^{L,+} | \hat{j}_x | \psi_{eq}^{L,+} \rangle} \right| |t_{\eta\sigma}^{ee}|^2 + \left| \frac{\langle \psi_{hq}^{R,+} | \hat{j}_x | \psi_{hq}^{R,+} \rangle}{\langle \psi_{eq}^{L,+} | \hat{j}_x | \psi_{eq}^{L,+} \rangle} \right| |t_{\eta\sigma}^{he}|^2 + \left| \frac{\langle \psi_{hq}^{R,+} | \hat{j}_x | \psi_{hq}^{R,+} \rangle}{\langle \psi_{hq}^{L,+} | \hat{j}_x | \psi_{hq}^{L,+} \rangle} \right| |t_{\eta\sigma}^{hh}|^2, \quad (7)$$

where the particle current density operator $\hat{j}_x \equiv \frac{-i}{\hbar} [x, H_{\text{BdG}}] = \eta v_F v_z \tau_x$, with v_z the Pauli matrix operating in the Nambu space.

We notice that the phonon contribution to the thermal transport can be profoundly suppressed by the mismatch in vibrational properties of the superconducting and magnetic regions [27,68,69]. Therefore, we only concentrate on thermal conductance contributed by electronlike and holelike quasiparticles and neglect the contribution from phonons. In terms of the transmission probability $\mathcal{T}_{\eta\sigma}(\epsilon, \theta)$, the heat current can be written as [9–22,27]

$$J = \frac{1}{h} \sum_{\eta\sigma} \int_{\Delta(T)}^{\infty} d\epsilon \int_{-\pi/2}^{\pi/2} \cos \theta d\theta \epsilon \mathcal{T}_{\eta\sigma}(\epsilon, \theta) \times [f(\epsilon, T_L) - f(\epsilon, T_R)], \quad (8)$$

where the Fermi distribution function $f(\epsilon, T_{L(R)}) = [e^{\epsilon/(k_B T_{L(R)})} + 1]^{-1}$ and $\Delta(T) = \max(\Delta_L(T_L), \Delta_R(T_R))$.

For the temperature bias $\delta T \rightarrow 0$, the thermal conductance in the linear response regime can be defined as $\tilde{\kappa} = (J/\delta T)_{\delta T \rightarrow 0}$, and which can be reformulated as

$$\tilde{\kappa} = \frac{1}{h} \sum_{\eta\sigma} \int_{\Delta(T)}^{\infty} d\epsilon \int_{-\pi/2}^{\pi/2} \frac{\mathcal{T}_{\eta\sigma}(\epsilon, \theta) \epsilon^2 \cos \theta d\theta}{4k_B T^2 \cosh^2\left(\frac{\epsilon}{2k_B T}\right)}. \quad (9)$$

To normalize the thermal conductance, it is convenient to introduce a quantity of $\kappa_0 = 4\pi^2 k_B^2 T / (3h)$, where $\pi^2 k_B^2 T / (3h)$ is the thermal conductance quantum [70] and the factor 4 takes into account the valley and spin indices. In doing so, the normalized thermal conductance can be expressed as $\kappa = \tilde{\kappa} / \kappa_0$.

III. RESULTS AND DISCUSSION

In this section, we proceed to analyze the numerical results and concentrate in particular on the manifestations of the perpendicular electric field in the thermal conductance. Without loss of generality, we choose silicene as a prototype of BTDM with $\lambda_{\text{SO}} = 3.9$ meV [39]. Considering that the typical value of the superconducting gap magnitude is of the order of ~ 1 meV [50–54,59–61], we take $\Delta_0 = 0.2\lambda_{\text{SO}}$ in the numerical calculation. The superconducting coherence length is defined as $\xi = \hbar v_F / \Delta_0$. To ensure the validity of the model described in Eq. (1), we set $\mu_S = 100\lambda_{\text{SO}}$ to satisfy $\mu_S \gg \Delta(T)$ and retain the relationship of $\mu_S \gg \mu_M$ throughout this work. In doing so, the quasiparticle scattering angles in the superconducting regions turn to $\theta_{eq,hq}^{L,R} \simeq 0$ and the relevant scattering events reduce into one-dimensional scenarios, similar to the studies reported in Refs. [11–14,22]. The employed potential profile under the condition of $\mu_S \gg \mu_M$ are oversimplifications, since in practice there may exist

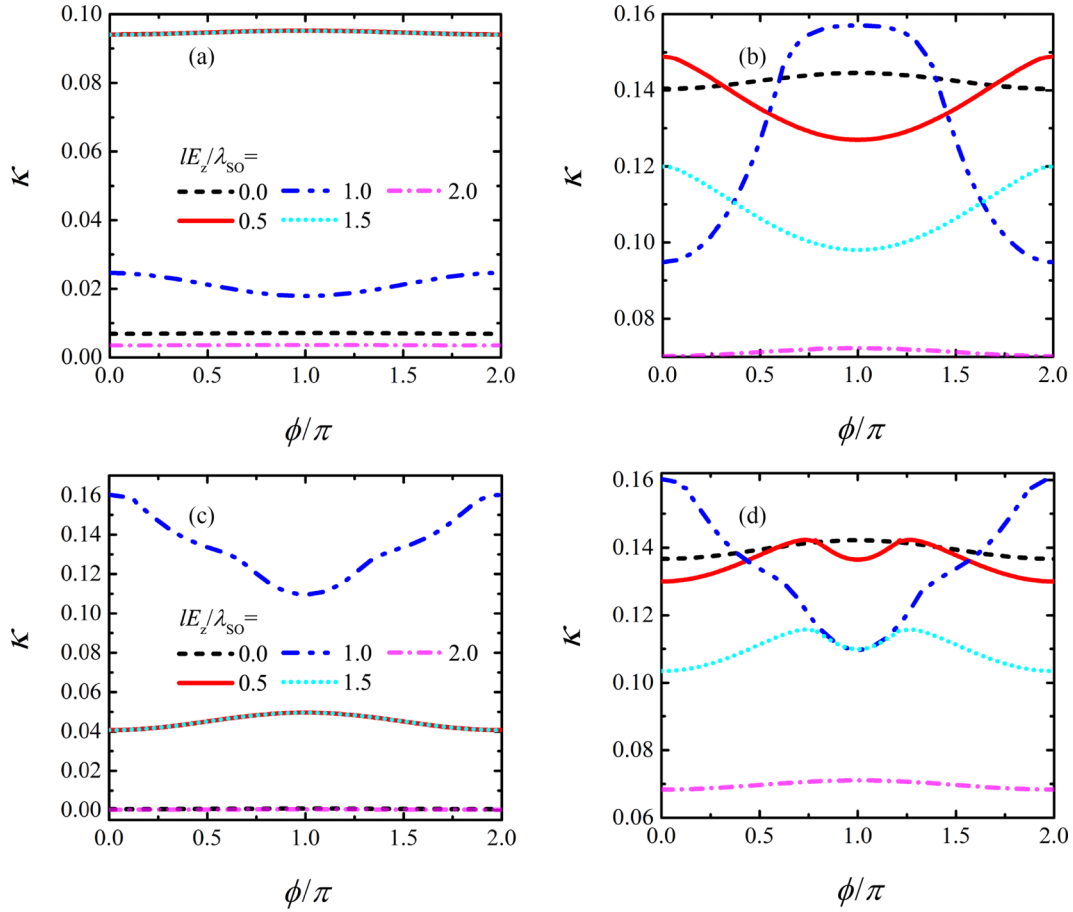


FIG. 2. Phase-difference-dependent normalized thermal conductance with different perpendicular electric fields, where $\mu_M = 0$ in (a) and (c), and $\mu_M = \lambda_{SO}$ in (b) and (d). Panels (a) and (b) and panels (c) and (d) present the results in the S-AF-S junction with $h_{AF} = 0.4\lambda_{SO}$ and the S-F-S junction with $h_F = 0.4\lambda_{SO}$, respectively. In all panels, $d = \xi$ and $T = T_C/2$.

charge redistributions which can alter the quantity of μ_M and smoothen the potential profile to deviate from the rectangular potential barrier. While the consequences caused by the charge redistributions may quantitatively change the thermal conductance, the physical picture and main results on the electrical tunability of phase-coherent thermal conductance should remain valid. To be more specific, in the M regions of S-AF-S and S-F-S junctions only the branches with band edges approaching the regime of $[-\Delta(T), \Delta(T)]$ can dominate the thermal transport, thus the electrical tunability of phase-coherent thermal conductance is rooted in the electrically controllable band edges of M regions, which will be further elucidated later. Since the band edges can also be regulated by the exchange field, even in the presence of local variations in the chemical potential μ_M , by appropriately setting the exchange field the band edges can always be modulated by the perpendicular electric field to be inside or outside of the regime of $[-\Delta(T), \Delta(T)]$ to achieve the electrically tunable phase-coherent thermal conductance. Additionally, in this work we are not interested in the effects of the interfacial potential barriers on the thermal conductance and single out $Z_L = Z_R = \pi$ throughout the paper, since the influences of interfacial potential barriers on the superconducting coherent transport have been intensively investigated [14,27,55,58]. It

is well known that the transmission probability and resulting conductance periodically oscillate with respect to $Z_{L,R}$ without decaying profiles; this phenomenon is a typical hallmark of the momentum-spin/pseudospin locking in Dirac materials.

As a starting point, we focus on the effects of the perpendicular electric field on the phase-coherent thermal conductance. Figure 2 presents the ϕ -dependent thermal conductance with different perpendicular electric fields. As can be seen, in all cases the thermal conductance can be effectively modulated by the perpendicular electric field. Specifically, in the S-AF-S junction, by varying the strength of perpendicular electric field, the ϕ -dependent thermal conductance exhibits transitions between minimal and maximal values at $\phi = \pi$, as shown in Figs. 2(a) and 2(b). In the S-F-S junction, as depicted in Figs. 2(c) and 2(d), the perpendicular electric field changes the value of ϕ corresponding to the maximal and/or minimal thermal conductance, thereby significantly tailoring the pattern of ϕ -dependent thermal conductance. The electrical tunability of the phase-coherent thermal conductance results from the $|E_z$ -dependent band structures of BTDMs. Resorting to Eq. (1), in the M regions of S-AF-S and S-F-S junctions, the electronlike (holelike) band edges can be, respectively, formulated as $E_{\eta,\sigma}^{\pm,e(h)} = \pm(\mp)|E_z - \eta\sigma\lambda_{SO} - (+)\sigma h_{AF} - (+)\mu_M$ and $\varepsilon_{\eta,\sigma}^{\pm,e(h)} = \pm(\mp)|E_z - \eta\sigma\lambda_{SO}| - \sigma h_F - (+)\mu_M$, with the

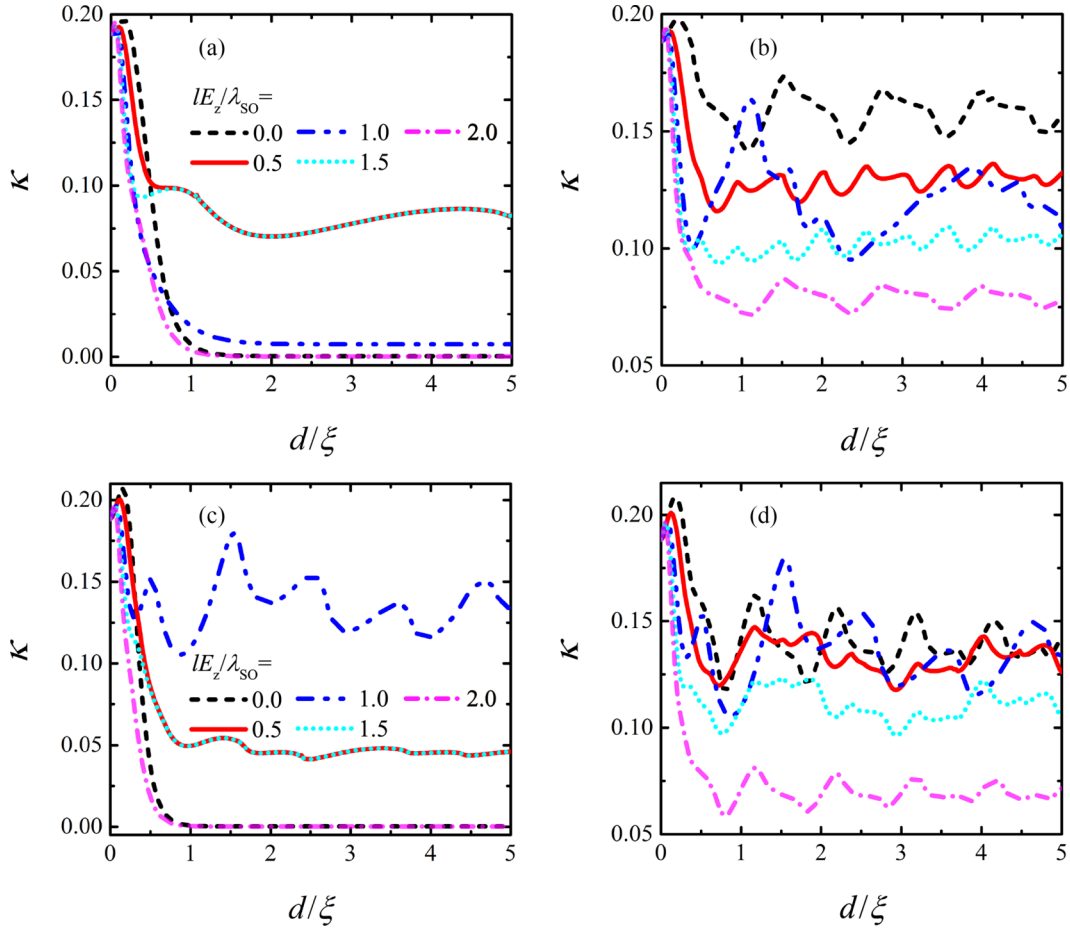


FIG. 3. Normalized thermal conductance κ as a function of the junction length d , where $\mu_M = 0$ in (a) and (c), and $\mu_M = \lambda_{SO}$ in (b) and (d). Panels (a) and (b) and panels (c) and (d) present the scenarios in the S-AF-S junction with $h_{AF} = 0.4\lambda_{SO}$ and S-F-S junction with $h_F = 0.4\lambda_{SO}$, respectively. In all panels, $\phi = \pi$ and $T = T_C/2$.

conduction (valence) band edge being indicated by the superscript $+(-)$ of $E_{\eta,\sigma}^{\pm,e(h)}$ and $\varepsilon_{\eta,\sigma}^{\pm,e(h)}$. Accordingly, in both junctions the perpendicular electric field IE_z can effectively tune the band edges which, in turn, regulate the band gaps of M regions. Since the quasiparticle transmission probabilities are profoundly influenced by the band gaps, the phase dependence of thermal conductance can be controlled by the perpendicular electric field. We point out that the electrical tunability of the phase-coherent thermal conductance results from the unique buckled sublattice structures of BTDMs and is absent in similar conventional [11,12,23–26] and topological Josephson junctions [9,10,13–21]. Moreover, we address that in our model owing to the unique buckled sublattice structures of BTDMs, the perpendicular electric fields can effectively tune the phase-coherent thermal conductance by modulating the band structures of M regions, rather than the pairing symmetries of superconducting regions. In this sense, we expect that the physical picture and main results on the electrical tunability of phase-coherent thermal conductance still hold for other types of pairing symmetries. In addition, the configurations of ϕ -dependent thermal conductance strongly depend on the type of exchange field and on the chemical potential μ_M . We will illustrate the underlying physics in terms of the band structures of M regions.

Since the thermal conductance is essentially contributed by the propagating quasiparticles with energies just above the superconducting gap [14,23–26], in the M region of S-AF-S (S-F-S) only the branches with band edges satisfying $E_{\eta,\sigma}^{+(-),e(h)} \leq \Delta(T)$ ($\varepsilon_{\eta,\sigma}^{+(-),e(h)} \leq \Delta(T)$) or $E_{\eta,\sigma}^{-(+),e(h)} \geq -\Delta(T)$ ($\varepsilon_{\eta,\sigma}^{-(+),e(h)} \geq -\Delta(T)$) can dominate the thermal transport. Keeping this principle in mind, we first discuss the scenarios in the S-AF-S junction with a undoped M region, i.e., $\mu_M = 0$. According to the parameters fixed in Figs. 2 and 3, in the situations of $IE_z = 0$, λ_{SO} , and $2\lambda_{SO}$, all band edges are outside of the regime of $[-\Delta(T), \Delta(T)] \simeq [-0.2\lambda_{SO}, 0.2\lambda_{SO}]$, so that the thermal transport is determined by the evanescent quasiparticles. Consequently, as shown in Fig. 3(a), the thermal conductance exponentially decays by increasing the junction length for $IE_z = 0$, λ_{SO} , and $2\lambda_{SO}$. When the junction length $d = \xi$ is large enough [see Fig. 3(a)], the thermal conductance dictated by the evanescent quasiparticles is strongly suppressed in the cases of $IE_z = 0$, λ_{SO} , and $2\lambda_{SO}$, as depicted in Fig. 2(a). While for $IE_z = 0.5\lambda_{SO}$ and $1.5\lambda_{SO}$, there are two branches with band edges being located in the regime of $[-\Delta(T), \Delta(T)]$, i.e., $E_{-1,-1}^{\pm,e}|_{IE_z=0.5\lambda_{SO}} = E_{+1,+1}^{\mp,h}|_{IE_z=0.5\lambda_{SO}} = \pm 0.1\lambda_{SO}$ and $E_{+1,+1}^{\pm,e}|_{IE_z=1.5\lambda_{SO}} = E_{-1,-1}^{\mp,h}|_{IE_z=1.5\lambda_{SO}} = \pm 0.1\lambda_{SO}$, respectively.

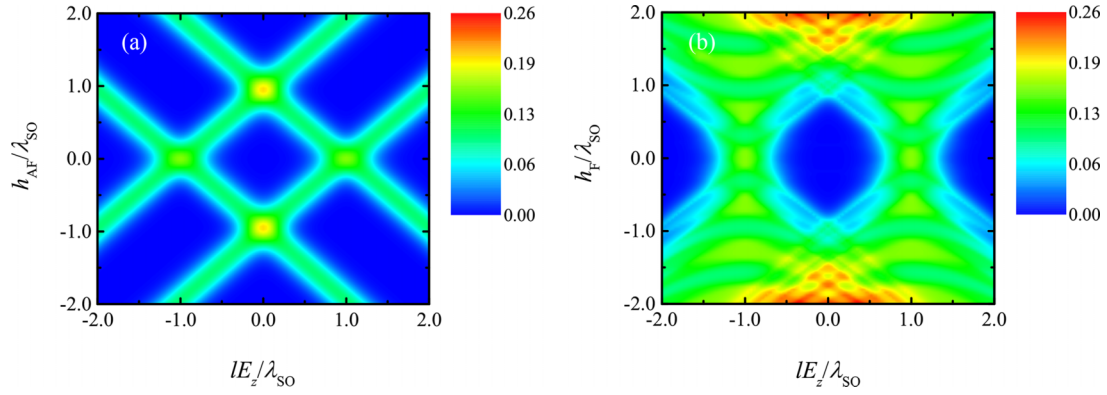


FIG. 4. Contour plots of the normalized thermal conductance κ of (a) S-AF-S junction and (b) S-F-S junction, where $\phi = \pi$, $d = \xi$, $\mu_M = 0$, and $T = T_C/2$.

Therefore, in the situation of $|E_z| = 0.5\lambda_{SO}$ ($1.5\lambda_{SO}$), the thermal conductance is mainly contributed by the spin-down (spin-up) electronlike propagating quasiparticles of K' (K) valley and the spin-up (spin-down) holelike propagating quasiparticles stemming from K (K') valley, as manifested by the oscillating profile of d -dependent thermal conductance shown in Fig. 3(a). When the M region is lightly doped with $\mu_M = \lambda_{SO}$, for each value of $|E_z|$ selected in Figs. 2 and 3, there exist at least two branches that can approach in the regime of $[-\Delta(T), \Delta(T)]$ to support propagating quasiparticles. As a showcase, for $|E_z| = 2\lambda_{SO}$ the band edges $E_{+1,+1}^{+,e}|_{|E_z|=2\lambda_{SO}} = -0.4\lambda_{SO} < \Delta(T)$ and $E_{-1,-1}^{+,h}|_{|E_z|=2\lambda_{SO}} = 0.4\lambda_{SO} > -\Delta(T)$, thus both the spin-up electronlike branch of K valley and the spin-down holelike branch of K' valley can support propagating quasiparticles. As shown in Fig. 3(b), the thermal conductance exhibits pronounced oscillating profiles with respect to the junction length.

In the S-F-S junction, the dependence of the phase-coherent thermal conductance on $|E_z|$ can be analyzed in the similar way mentioned above. Here we only concentrate on the distinct scenarios that are absent in the S-AF-S junction. In the S-F-S junction, although the band edges of M region rely on the ferromagnetic exchange field h_F , the band gap scales $\delta_{\eta,\sigma}^{F,e} = \delta_{\eta,\sigma}^{F,h} = 2|E_z - \eta\sigma\lambda_{SO}|$ are independent of h_F , in contrast to the manifestation of antiferromagnetic exchange field in the S-AF-S junction. Therefore, for a set of fixed valley and spin indices, the band gap in the M region of S-F-S junction is solely determined by the perpendicular electric field. This character leads to intriguing consequences in the special case of $|E_z| = \lambda_{SO}$, where the branches with $(\eta, \sigma) = (+1, +1)$ and $(\eta, \sigma) = (-1, -1)$ are gapless, thus the spin-up quasiparticles originating from K valley and the spin-down quasiparticles emanating from K' valley invariably dominate the thermal transport. Consequently, when $|E_z| = \lambda_{SO}$ the thermal conductance obviously oscillates with d , regardless of the values of μ_M , as shown in Figs. 3(c) and 3(d).

To further elucidate the different manifestations of antiferromagnetic and ferromagnetic exchange fields in the thermal transport, in Fig. 4 we present the contour plots of the normalized thermal conductance in the parameter plane $(|E_z|, h)$ with $\mu_M = 0$. In the S-AF-S junction, the

antiferromagnetic exchange field regulates not only the band edges, but also the gap scales as $\delta_{\eta,\sigma}^{AF,e(h)} = 2|E_z - \eta\sigma\lambda_{SO} - (+)\sigma h_{AF}|$. Since the band gap of M region depends both on the antiferromagnetic exchange field and on the perpendicular electric field, in the $(|E_z|, h_{AF})$ plane the nonvanishing thermal conductance can only appear in the regions delimited by the conditions of $\pm h_{AF} + 0.8\lambda_{SO} \leq |E_z| \leq \pm h_{AF} + 1.2\lambda_{SO}$ and $\pm h_{AF} - 1.2\lambda_{SO} \leq |E_z| \leq \pm h_{AF} - 0.8\lambda_{SO}$, as shown in Fig. 4(a). In the S-F-S junction, by contrast, the ferromagnetic exchange field only shifts the position, rather than the scale of band gap. For a given choice of spin and valley indices, the band gaps of electronlike and holelike branches share the same value, i.e., $\delta_{\eta,\sigma}^{F,e} = \delta_{\eta,\sigma}^{F,h} = 2|E_z - \eta\sigma\lambda_{SO}|$. Therefore, in the case of $|E_z| = \pm\lambda_{SO}$ both the electronlike and holelike branches with $\eta\sigma = \pm(-)1$ are gapless to support propagating quasiparticles, regardless of the value of h_F . As presented by Fig. 4(b), in the whole range of h_F the thermal conductance keeps finite at $|E_z| = \pm\lambda_{SO}$; this character is quite distinct from that of S-AF-S junction. Furthermore, since the ferromagnetic exchange field can shift the positions of band gaps without affecting their scales, the band gaps can be pushed outside of the regime of $[-\Delta(T), \Delta(T)]$ when the ferromagnetic field is large enough. As a consequence, in the whole range of $|E_z|$ the thermal conductance is nonvanishing when $|h_F| \gtrsim \lambda_{SO}$, visibly differing from that in the S-AF-S junction.

IV. CONCLUSION

In conclusion, we have theoretically studied the thermal transport properties in BTDM-based S-AF-S and S-F-S junctions by virtue of the scattering wave approach. We have revealed that, in both S-AF-S and S-F-S junctions, the phase dependence of thermal conductance can be effectively controlled by perpendicular electric fields. This scenario is rooted in the exotic buckled sublattice geometries of BTDMs and is absent in similar conventional and topological Josephson junctions. Resorting to the band structures of M regions, we have illustrated the underlying mechanism behind the electrical tunability of thermal conductance. The different influences of the antiferromagnetic and ferromagnetic exchange fields on the thermal conductance have also been elucidated in detail. These findings suggest that the BTDM-based Josephson

junctions provide unique platforms for obtaining electrically tunable phase-coherent thermal transport, and we anticipate more interesting results for the thermal transport properties regarding the crossed Andreev reflections in BTDM-based superconducting hybrid structures.

ACKNOWLEDGMENTS

We acknowledge helpful discussions with R. Wang. This work was supported by the Science and Technology Planning Project of Hunan Province (Grant No. 2019RS2033), the National Natural Science Foundation of China (Grants No. 11804091 and No. U2001215), the Hunan Provincial Natural Science Foundation (Grant No. 2019JJ50380), and the excellent youth fund of the Hunan Provincial Education Department (Grant No. 18B014).

APPENDIX: CALCULATION OF THE BASIS SCATTERING STATES IN BTDM-BASED S-AF-S AND S-F-S JUNCTIONS

In this Appendix we give necessary calculation details regarding the wave functions and related parameters in the BTDM-based S-AF-S and S-F-S junctions.

We assume that the translational symmetry is preserved in the y direction of the proposed setup, so that the transverse momentum k_y can be treated as a good quantum number. Under this assumption, in the S regions solving the BdG equation $\mathcal{H}(-i\partial_x, k_y)\psi = \epsilon\psi$ straightforwardly yields

$$\psi_{eq}^{L(R),\pm} = \begin{pmatrix} \pm\eta\sigma e^{\pm i\eta\theta_{eq}^{L(R)}} u^{L(R)} \\ \sigma\gamma_{eq}^{L(R)} u^{L(R)} \\ \pm\eta e^{\pm i\eta\theta_{eq}^{L(R)} - i\phi_{L(R)}} v^{L(R)} \\ \gamma_{eq}^{L(R)} e^{-i\phi_{L(R)}} v^{L(R)} \end{pmatrix} e^{\pm ik_{eq}^{L(R)} \cos\theta_{eq}^{L(R)} x}, \quad (\text{A1a})$$

$$\psi_{hq}^{L(R),\pm} = \begin{pmatrix} \mp\eta\sigma e^{\mp i\eta\theta_{hq}^{L(R)}} v^{L(R)} \\ \sigma\gamma_{hq}^{L(R)} v^{L(R)} \\ \mp\eta e^{\mp i\eta\theta_{hq}^{L(R)} - i\phi_{L(R)}} u^{L(R)} \\ \gamma_{hq}^{L(R)} e^{-i\phi_{L(R)}} u^{L(R)} \end{pmatrix} e^{\mp ik_{hq}^{L(R)} \cos\theta_{hq}^{L(R)} x}, \quad (\text{A1b})$$

where we omit the trivial factor $e^{ik_y y}$, and the involved parameters take the forms of

$$k_{eq}^{L,R} = \sqrt{(\mu_S + (-)\text{sgn}(\epsilon)\sqrt{\epsilon^2 - \Delta_{L,R}^2(T_{L,R})})^2 - m_{\eta\sigma}^2}/(\hbar v_F), \quad (\text{A2a})$$

$$\gamma_{eq}^{L,R} = (\sqrt{(\hbar v_F k_{eq}^{L,R})^2 + m_{\eta\sigma}^2} - m_{\eta\sigma})/(\hbar v_F k_{eq}^{L,R}), \quad (\text{A2b})$$

$$\theta_{eq}^{L,R} = \sin^{-1}(k_y/k_{eq}^{L,R}), \quad (\text{A2c})$$

$$u^{L,R} = \sqrt{\frac{1}{2}(1 + \sqrt{1 - \Delta_{L,R}^2(T_{L,R})/\epsilon^2})}, \quad (\text{A2d})$$

$$v^{L,R} = \text{sgn}(\epsilon)\sqrt{\frac{1}{2}(1 - \sqrt{1 - \Delta_{L,R}^2(T_{L,R})/\epsilon^2})}. \quad (\text{A2e})$$

In the magnetic region ($0 < x < d$), after omitting the trivial factor $e^{ik_y y}$, the scattering states can be formulated as

$$\psi_e^\pm = \begin{pmatrix} \pm\eta s_e e^{\pm i\eta s_e \alpha_e} \\ \gamma_e \\ 0 \\ 0 \end{pmatrix} e^{\pm i s_e k_e \cos\alpha_e x}, \quad (\text{A3a})$$

$$\psi_h^\pm = \begin{pmatrix} 0 \\ 0 \\ \mp\eta s_h e^{\pm i\eta s_h \alpha_h} \\ \gamma_h \end{pmatrix} e^{\pm i s_h k_h \cos\alpha_h x}, \quad (\text{A3b})$$

where the scattering angle $\alpha_{e(h)} = \sin^{-1}(k_y/k_{e(h)})$.

In the S-AF-S junction, the related parameters in Eq. (A3) are given by

$$k_{e(h)} = \sqrt{(\epsilon + (-)\mu_M)^2 - (m_{\eta\sigma} - (+)\sigma h_{AF})^2}/(\hbar v_F), \quad (\text{A4a})$$

$$\gamma_{e(h)} = (\epsilon + (-)\mu_M - (+)m_{\eta\sigma} + \sigma h_{AF})/(\hbar v_F k_{e(h)}), \quad (\text{A4b})$$

$$s_{e(h)} = \text{sgn}(\epsilon - |m_{\eta\sigma} - (+)\sigma h_{AF}| + (-)\mu_M). \quad (\text{A4c})$$

While in the S-F-S junction, the corresponding parameters in Eq. (A3) are defined as

$$k_{e(h)} = \sqrt{(\epsilon + (-)\mu_M + \sigma h_F)^2 - m_{\eta\sigma}^2}/(\hbar v_F), \quad (\text{A5a})$$

$$\gamma_{e(h)} = [\epsilon + (-)\mu_M - (+)m_{\eta\sigma} + \sigma h_F]/(\hbar v_F k_{e(h)}), \quad (\text{A5b})$$

$$s_{e(h)} = \text{sgn}(\epsilon - |m_{\eta\sigma}| + (-)\mu_M + \sigma h_F). \quad (\text{A5c})$$

- [1] J. P. Pekola and B. Karimi, *Rev. Mod. Phys.* **93**, 041001 (2021).
- [2] F. Giazotto and M. J. Martínez-Pérez, *Nature (London)* **492**, 401 (2012).
- [3] A. Fornieri, C. Blanc, R. Bosisio, S. D'Ambrosio, and F. Giazotto, *Nat. Nanotechnol.* **11**, 258 (2016).
- [4] G. F. Timossi, A. Fornieri, F. Paolucci, C. Puglia, and F. Giazotto, *Nano Lett.* **18**, 1764 (2018).
- [5] A. Fornieri, G. Timossi, P. Virtanen, P. Solinas, and F. Giazotto, *Nat. Nanotechnol.* **12**, 425 (2017).

- [6] A. Fornieri and F. Giazotto, *Nat. Nanotechnol.* **12**, 944 (2017).
- [7] C. D. Shelly, E. A. Matrozova, and V. T. Petrashov, *Sci. Adv.* **2**, e1501250 (2016).
- [8] A. G. Bauer and B. Sothmann, *Phys. Rev. B* **104**, 195418 (2021).
- [9] L. Bours, B. Sothmann, M. Carrega, E. Strambini, A. Braggio, E. M. Hankiewicz, L. W. Molenkamp, and F. Giazotto, *Phys. Rev. Appl.* **11**, 044073 (2019).

- [10] A. Mukhopadhyay and S. Das, *Phys. Rev. B* **106**, 075421 (2022).
- [11] F. Hajiloo, F. Hassler, and J. Splettstoesser, *Phys. Rev. B* **99**, 235422 (2019).
- [12] S. S. Pershoguba and L. I. Glazman, *Phys. Rev. B* **99**, 134514 (2019).
- [13] B. Sothmann, F. Giazotto, and E. M. Hankiewicz, *New J. Phys.* **19**, 023056 (2017).
- [14] B. Sothmann and E. M. Hankiewicz, *Phys. Rev. B* **94**, 081407(R) (2016).
- [15] A. G. Bauer, B. Scharf, L. W. Molenkamp, E. M. Hankiewicz, and B. Sothmann, *Phys. Rev. B* **104**, L201410 (2021).
- [16] A. Mukhopadhyay and S. Das, *Phys. Rev. B* **103**, 144502 (2021).
- [17] D. Gresta, G. Blasi, F. Taddei, M. Carrega, A. Braggio, and L. Arrachea, *Phys. Rev. B* **103**, 075439 (2021).
- [18] L. Bours, B. Sothmann, M. Carrega, E. Strambini, E. M. Hankiewicz, L. W. Molenkamp, and F. Giazotto, *Phys. Rev. Appl.* **10**, 014027 (2018).
- [19] G. Blasi, F. Taddei, L. Arrachea, M. Carrega, and A. Braggio, *Phys. Rev. Lett.* **124**, 227701 (2020).
- [20] H. Li and Y. Y. Zhao, *J. Phys.: Condens. Matter* **29**, 465001 (2017).
- [21] S. J. Wang and Z. P. Niu, *Phys. Lett. A* **448**, 128333 (2022).
- [22] A. G. Bauer and B. Sothmann, *Phys. Rev. B* **99**, 214508 (2019).
- [23] K. Maki and A. Griffin, *Phys. Rev. Lett.* **15**, 921 (1965).
- [24] G. D. Guttman, B. Nathanson, E. Ben-Jacob, and D. J. Bergman, *Phys. Rev. B* **55**, 3849 (1997).
- [25] E. Zhao, T. Löfwander, and J. A. Sauls, *Phys. Rev. Lett.* **91**, 077003 (2003).
- [26] E. Zhao, T. Löfwander, and J. A. Sauls, *Phys. Rev. B* **69**, 134503 (2004).
- [27] J. Ren and J.-X. Zhu, *Phys. Rev. B* **87**, 165121 (2013).
- [28] J. Zheng, Y. Xiang, C. Li, R. Yuan, F. Chi, and Y. Guo, *Phys. Rev. Appl.* **14**, 034027 (2020).
- [29] J. Zhao, H. Liu, Z. Yu, R. Quhe, S. Zhou, Y. Wang, C. C. Liu, H. Zhong, N. Han, J. Lu, Y. Yao, and K. Wu, *Prog. Mater. Sci.* **83**, 24 (2016).
- [30] M. X. Chen, Z. Zhong, and M. Weinert, *Phys. Rev. B* **94**, 075409 (2016).
- [31] D. Chiappe, E. Scalise, E. Cinquanta, C. Grazianetti, B. van den Broek, M. Fanciulli, M. Houssa, and A. Molle, *Adv. Mater.* **26**, 2096 (2014).
- [32] C. Grazianetti, S. De Rosa, C. Martella, P. Targa, D. Codegoni, P. Gori, O. Pulci, A. Molle, and S. Lupi, *Nano Lett.* **18**, 7124 (2018).
- [33] F. B. Wiggers, A. Fleurence, K. Aoyagi, T. Yonezawa, Y. Yamada-Takamura, H. Feng, J. Zhuang, Y. Du, A. Y. Kovalgin, and M. P. de Jong, *2D Mater.* **6**, 035001 (2019).
- [34] Z. Ben Jabra, M. Abel, F. Fabbri, J.-N. Aqua, M. Koudia, A. Michon, P. Castrucci, A. Ronda, H. Vach, M. De Crescenzi, and I. Berbezier, *ACS Nano* **16**, 5920 (2022).
- [35] A. Molle, J. Goldberger, M. Houssa, Y. Xu, S.-C. Zhang, and D. Akinwande, *Nat. Mater.* **16**, 163 (2017).
- [36] P. Gori, I. Kupchak, F. Bechstedt, D. Grassano, and O. Pulci, *Phys. Rev. B* **100**, 245413 (2019).
- [37] B. Feng, H. Zhou, Y. Feng, H. Liu, S. He, I. Matsuda, L. Chen, E. F. Schwier, K. Shimada, S. Meng, and K. Wu, *Phys. Rev. Lett.* **122**, 196801 (2019).
- [38] R. Y. Kezerashvili and A. Spiridonova, *Phys. Rev. B* **103**, 165410 (2021).
- [39] C.-C. Liu, H. Jiang, and Y. Yao, *Phys. Rev. B* **84**, 195430 (2011).
- [40] N. D. Drummond, V. Zólyomi, and V. I. Fal'ko, *Phys. Rev. B* **85**, 075423 (2012).
- [41] W. F. Tsai, C. Y. Huang, T. R. Chang, H. Lin, H. T. Jeng, and A. Bansil, *Nat. Commun.* **4**, 1500 (2013).
- [42] C.-H. Chen, W.-W. Li, Y.-M. Chang, C.-Y. Lin, S.-H. Yang, Y. Xu, and Y.-F. Lin, *Phys. Rev. Appl.* **10**, 044047 (2018).
- [43] J. G. Rojas-Briseño, M. A. Flores-Carranza, P. Villasana-Mercado, S. Molina-Valdovinos, and I. Rodríguez-Vargas, *Phys. Rev. B* **103**, 155431 (2021).
- [44] W.-T. Lu, Q.-F. Sun, H.-Y. Tian, B.-H. Zhou, and H.-M. Liu, *Phys. Rev. B* **102**, 125426 (2020).
- [45] Z. P. Niu, *New J. Phys.* **21**, 093044 (2019).
- [46] T. Yokoyama, *Phys. Rev. B* **87**, 241409(R) (2013).
- [47] M. Moun and G. Sheet, *Supercond. Sci. Technol.* **35**, 083001 (2022).
- [48] M. Ezawa, *J. Supercond. Novel Magn.* **28**, 1249 (2015).
- [49] Y. Wei, T. Liu, C. Huang, Y. C. Tao, and F. Qi, *Phys. Rev. Res.* **3**, 033131 (2021).
- [50] J. Linder and T. Yokoyama, *Phys. Rev. B* **89**, 020504(R) (2014).
- [51] D. Frombach, S. Park, A. Schroer, and P. Recher, *Phys. Rev. B* **98**, 205305 (2018).
- [52] D. Kuzmanovski, J. Linder, and A. Black-Schaffer, *Phys. Rev. B* **94**, 180505 (2016).
- [53] H. Li, R. Wang, and C. S. Ting, *Phys. Rev. B* **94**, 085422 (2016).
- [54] X. Zhou and G. Jin, *Phys. Rev. B* **95**, 195419 (2017).
- [55] G. C. Paul and A. Saha, *Phys. Rev. B* **95**, 045420 (2017).
- [56] H. Li, *Phys. Rev. B* **94**, 075428 (2016).
- [57] W.-T. Lu and Q.-F. Sun, *Phys. Rev. B* **104**, 045418 (2021).
- [58] G. C. Paul, S. Sarkar, and A. Saha, *Phys. Rev. B* **94**, 155453 (2016).
- [59] H. B. Heersche, P. Jarillo-Herrero, J. B. Oostinga, L. M. K. Vandersypen, and A. F. Morpurgo, *Nature (London)* **446**, 56 (2007).
- [60] L. Bretheau, J. I.-J. Wang, R. Pisoni, K. Watanabe, T. Taniguchi, and P. Jarillo-Herrero, *Nat. Phys.* **13**, 756 (2017).
- [61] D. Perconte, F. A. Cuellar, C. Moreau-Luchaire, M. Piquemal-Banci, R. Galceran, P. R. Kidambi, M.-B. Martin, S. Hofmann, R. Bernard, B. Dlubak, P. Seneor, and J. E. Villegas, *Nat. Phys.* **14**, 25 (2018).
- [62] D. K. Efetov, L. Wang, C. Handschin, K. B. Efetov, J. Shuang, R. Cava, T. Taniguchi, K. Watanabe, J. Hone, C. R. Dean, and P. Kim, *Nat. Phys.* **12**, 328 (2016).
- [63] D. K. Efetov and K. B. Efetov, *Phys. Rev. B* **94**, 075403 (2016).
- [64] D. J. Trainer, B. Wang, F. Bobba, N. Samuelson, X. Xi, J. Zasadzinski, J. Nieminen, A. Bansil, and M. Iavarone, *ACS Nano* **14**, 2718 (2020).
- [65] P. Dreher, W. Wan, A. Chikina, M. Bianchi, H. Guo, R. Harsh, S. Mañas-Valero, E. Coronado, A. J. Martínez-Galera, P. Hofmann, J. A. Miwa, and M. M. Ugeda, *ACS Nano* **15**, 19430 (2021).

- [66] A. M. Tokmachev, D. V. Averyanov, I. A. Karateev, O. E. Parfenov, O. A. Kondratev, A. N. Taldenkov, and V. G. Storchak, *Adv. Funct. Mater.* **27**, 1606603 (2017).
- [67] A. M. Tokmachev, D. V. Averyanov, O. E. Parfenov, A. N. Taldenkov, I. A. Karateev, I. S. Sokolov, O. A. Kondratev, and V. G. Storchak, *Nat. Commun.* **9**, 1672 (2018).
- [68] E. T. Swartz and R. O. Pohl, *Rev. Mod. Phys.* **61**, 605 (1989).
- [69] N. Li, J. Ren, L. Wang, G. Zhang, P. Hänggi, and B. Li, *Rev. Mod. Phys.* **84**, 1045 (2012).
- [70] K. Schwab, E. Henriksen, J. Worlock, and M. L. Roukes, *Nature (London)* **404**, 974 (2000).